Cancer Cell
Article

Autologous Chemotaxis as a Mechanism of Tumor Cell Homing to Lymphatics via Interstitial Flow and Autocrine CCR7 Signaling

Jacqueline D. Shields,[1,3] Mark E. Fleury,[1,3] Carolyn Yong,[1] Alice A. Tomei,[1] Gwendalyn J. Randolph,[2] and Melody A. Swartz[1,*]
[1] Institute of Bioengineering, École Polytechnique Fédérale de Lausanne (EPFL), Lausanne 1015, Switzerland
[2] Department of Gene and Cell Medicine, Icahn Research Institute, Mount Sinai School of Medicine, New York, NY 10029, USA
[3] These authors contributed equally to this work.
*Correspondence: melody.swartz@epfl.ch
DOI 10.1016/j.ccr.2007.04.020

SUMMARY

CCR7 is implicated in lymph node metastasis of cancer, but its role is obscure. We report a mechanism explaining how interstitial flow caused by lymphatic drainage directs tumor cell migration by autocrine CCR7 signaling. Under static conditions, lymphatic endothelium induced CCR7-dependent chemotaxis of tumor cells through 3D matrices. However, interstitial flow induced strong increases in tumor cell migration that were also CCR7 dependent, but lymphatic independent. This autologous chemotaxis correlated with metastatic potential in four cell lines and was verified by visualizing directional polarization of cells in the flow direction. Computational modeling revealed that transcellular gradients of CCR7 ligand were created under flow to drive this response. This illustrates how tumor cells may be guided to lymphatics during metastasis.

INTRODUCTION

Although lymphatic metastasis is the major route of dissemination for many cancers (Chambers et al., 2002; Nathanson, 2003), the mechanisms underlying metastasis are unclear. It is suggested that more aggressive tumors induce lymphangiogenesis via secretion of lymphangiogenic growth factors (He et al., 2005; Mandriota et al., 2001; Skobe et al., 2001; Stacker et al., 2001), although evidence for tumor lymphangiogenesis, or the necessity of lymphangiogenesis for lymphatic metastasis, in human cancer remains controversial (Clarijs et al., 2001; Sipos et al., 2005; Williams et al., 2003; Wong et al., 2005).

Consistently, however, the occurrence of lymph node metastasis has been linked with expression of chemokine receptors, particularly CCR7 and CXCR4 (Arya et al., 2004; Darash-Yahana et al., 2004; Muller et al., 2001; Takeuchi et al., 2004). CCR7 is of particular interest since memory CD4+ T cells and dendritic cells, which constitutively traffic through lymphatics, require CCR7 for migration to lymph nodes (Debes et al., 2005; Forster et al., 1999; Ohl et al., 2004; Randolph et al., 2005). Cancer cells may exploit similar mechanisms to access the lymphatics: indeed, the incidence of lymph node metastases has been correlated with the presence of CCR7 on tissue sections of human cancers including breast cancer (Cabioglu et al., 2005) and melanoma (Takeuchi et al., 2004; Wiley et al., 2001) as well as colorectal (Gunther et al., 2005), head and neck (Wang et al., 2005), prostate (Heresi et al., 2005), non-small lung (Takanami, 2003), esophageal squamous cell (Ding et al., 2003), and gastric (Mashino et al., 2002) cancers. The known ligands for CCR7 are CCL21 and CCL19. CCL21 is expressed by lymphatic vessels (Gunn et al., 1998) and is secreted as a 12 kDa protein but is readily immobilized within extracellular matrix (ECM) by binding to sulfated proteoglycans (Patel

SIGNIFICANCE

Many cancers spread via the lymphatics, but the mechanisms used by tumor cells to access lymphatics remain unclear, although expression of the chemokine receptor CCR7 has been correlated with lymph node metastasis. We provide evidence that physiological levels of interstitial flow strongly enhance tumor cell polarization and migration. We show how tumor cells utilize interstitial flow to create and amplify autologous transcellular chemokine gradients and thus chemotact toward the draining lymphatic even when too far to sense any putative chemotactic signals from the lymphatic. This work also provides a twist to the well-described phenomenon of chemotaxis by showing that a cell can receive directional cues while at the same time being the source of such cues.

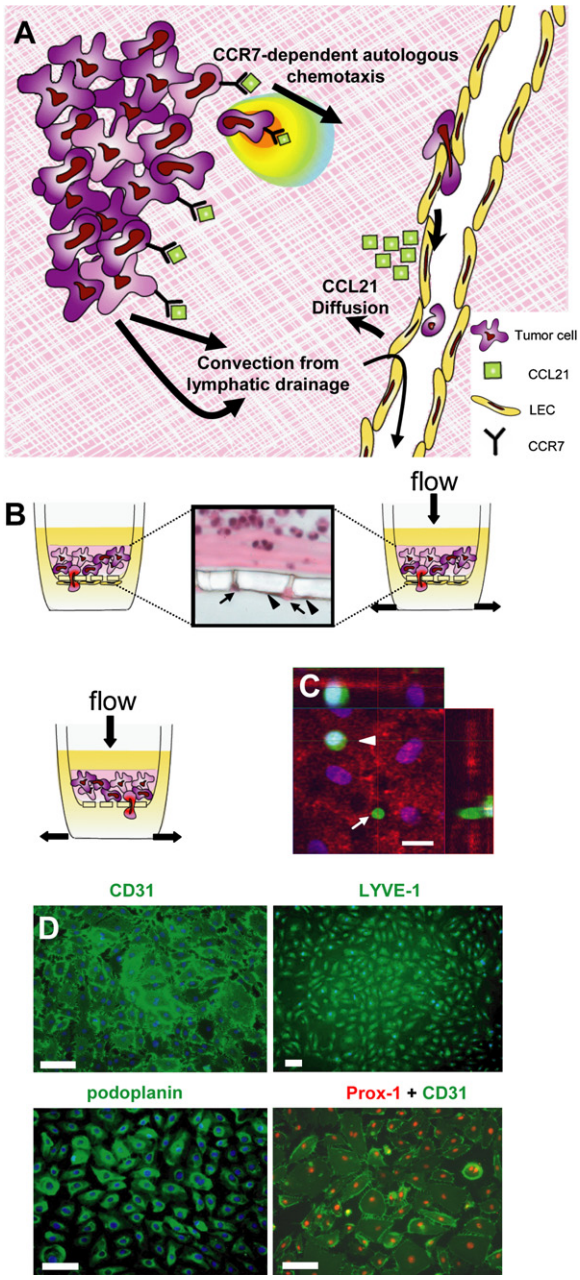

Figure 1. 3D Tissue Culture Model of the Tumor-Lymphatic Microenvironment

(A) Schematic of the tumor microenvironment where lymphatic vessels drain interstitial fluid, creating flow directed toward the lymphatic. This fluid convection promotes transport of signals from tumor to lymphatic but counteracts diffusive transport of signals from lymphatic to tumor, such as the lymphocyte homing chemokine CCL21. The potential role of CCR7-mediated autologous chemotaxis in this process is investigated here along with paracrine CCR7 signaling by lymphatics.

(B) Schematic of tissue culture model system incorporating a 3D extracellular matrix and interstitial flow to examine crosstalk between tumor cells and lymphatic endothelial cells (LECs) as well as the effects of flow on tumor cell migration, with and without LECs. Inset: Histological cross-section showing interface of tumor suspension, porous membrane, and LECs (arrowheads). Arrows indicate transmigrating tumor cells in membrane pores.

(C) Confocal image of the underside of the transwell membrane showing the lymphatic endothelial cell monolayer (CD31, red), one adhering tumor cell (GFP, green, arrowhead), and one tumor cell in the process of transmigration through a pore (arrow). Nuclei are shown in blue. Scale bar, 20 μm.

(D) Human dermal microvascular LECs as characterized by immunofluorescence for indicated markers. Scale bars, 100 μm.

et al., 2001). Similarly, CCL19 is secreted as an 8.8 kDa protein and is required for immunological functions including T cell priming and dendrite production by antigen-presenting cells, thereby affecting migratory properties (Randolph et al., 2005).

We suggest here a mechanism for CCR7-mediated tumor cell chemotaxis to lymphatics. In addition to sensing chemotactic gradients of CCL21/19 from lymphatics, we show that tumor cells also generate autologous gradients of CCR7 ligands by secreting them into the ECM under the influence of slow interstitial flow (IF). This mechanism uses the drainage function of lymphatics to direct tumor cells in a chemotactic manner toward lymphatic vessels serving the tumor, thus promoting tumor cell migration toward functional more than nonfunctional lymphatics. Furthermore, it is well established that tumors are highly vascularized and contain abnormally leaky capillaries (Jain, 2003, 2005; Carmeliet, 2003); tumor fluid flows through the interstitial space toward the draining lymphatics with a velocity of 0.1–0.8 μm/s (Chary and Jain, 1989; Dafni et al., 2002). This proposed mechanism follows from our recent computational demonstration that transcellular gradients of autocrine-secreted morphogen can form under IF (Fleury et al., 2006; Helm et al., 2005) in a 3D environment. The microenvironment created by normal lymphatic functioning in the space between the tumor margin and lymphatic vessel may similarly facilitate tumor migration toward lymphatics (Figure 1A).

We developed a simple in vitro 3D culture model to mimic this biophysical microenvironment and explore the interplay of IF and chemokine signaling between tumor cells and lymphatic endothelial cells (LECs; Figure 1B). Matrigel, a reconstituted ECM that is rich in sulfated proteoglycans (Kleinman and Martin, 2005), was used to facilitate chemokine interactions with the ECM and allow pericellular gradients of both tumor-secreted and LEC-secreted CCL21 to be established as they would in vivo. We show, using four different human cell lines (three breast and one melanoma), that tumor cells can create autocrine gradients of CCR7 ligands that guide their chemotaxis in the direction of flow (i.e., toward functional lymphatics). This occurs when a physiologic level of IF is present, even if LECs are absent, although the effect is greatly amplified when both IF and LECs are present. These findings introduce the mechanism of "autologous chemotaxis" for guiding tumor cells toward functional lymphatics and give mechanistic insight into why tumor CCR7 expression is correlated to lymph node metastasis. They suggest that CCR7 ligand secretion by tumor cells themselves, rather than or in addition to secretion by lymphatics, may be a potential target for preventing metastatic spread.

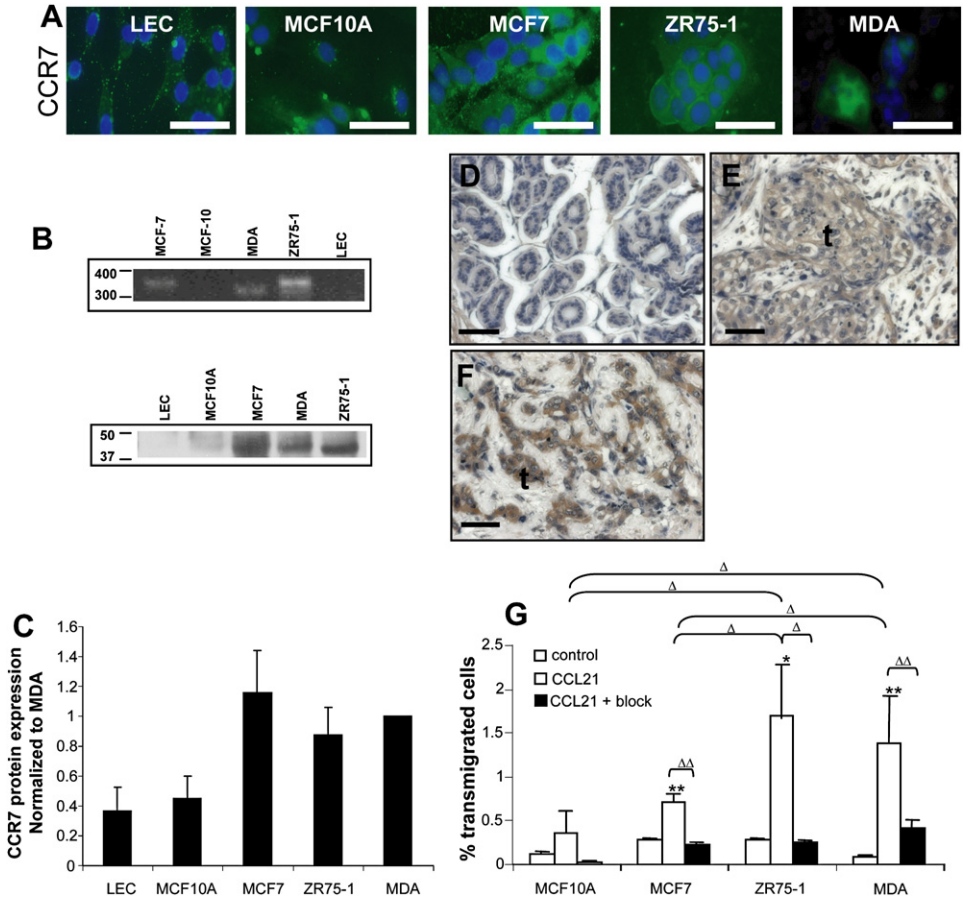

Figure 2. Tumor Cells Express Functional CCR7

(A) Immunofluorescence demonstrates CCR7 receptor expression in the three tumor cell lines, but very little in LECs or the nontumorigenic cell line MCF10A. Scale bar, 50 μm.

(B) Representative PCR (top) and Western blot (bottom) analysis again demonstrates CCR7 expression in tumor cells but not LECs or the nontumorigenic MCF10A.

(C) CCR7 band intensities from densitometry of Western blots (n = 3), normalized to expression in MDA cells.

(D–F) CCR7 expression (brown) in human breast tissue samples. Very low levels of CCR7 were detected in normal epithelial ductal tissue (D), while ductal carcinoma in situ (E) and invasive carcinoma (F) showed higher levels of CCR7 signal (tumor cells indicated by "t"). Scale bar, 50 μm.

(G) 3D chemoinvasion up a 4 ng/ml/μm CCL21 gradient of the four cell lines tested. MCF10A cells displayed a small but insignificant response to the CCL21 gradient, while the more invasive cell lines (ZR75-1 and MDA-MB-435S) showed substantial chemotaxis that could be abolished with neutralizing antibodies against CCL21 and CCR7 (*$p < 0.05$, **$p < 0.01$ compared with control [random migration in basal medium]; $^{\Delta}p < 0.05$, $^{\Delta\Delta}p < 0.01$ between other groups as indicated). Error bars represent mean ± SD.

RESULTS

Tumor Cell Expression of Functional CCR7

We examined a panel of four cell lines for the presence and functional response of CCR7, which included one nontumorigenic breast cell line, MCF10A (Soule et al., 1990), two breast tumor cell lines, MCF7 (Soule et al., 1990) and ZR75-1 (Engel et al., 1978), and one cell line of melanoma origin, MDA-MB-435S (Cailleau et al., 1978), which have low, moderate, and high metastatic potential, respectively. (We note that the MDA-MB-435S cell line was first characterized as a breast tumor cell line but was recently discovered to have melanoma origins [Rae et al., 2004, 2006; http://dtp.nci.nih.gov/docs/misc/common_files/mda-mb-435-update.html].) Immunofluorescence (Figure 2A) demonstrated strong CCR7 expression in the three tumor cell lines but weak staining in LECs and MCF10A cells; this was confirmed by Western blot and PCR (Figures 2B and 2C). Human breast cancer sections were consistent with the cell line expression: low levels of CCR7 were detected in normal breast ductal tissue (Figure 2D), while strong staining was observed in ductal carcinoma in situ (DCIS; Figure 2E) and invasive carcinoma (Figure 2F).

Furthermore, the three tumor cell lines, but not the benign cells, showed strong chemotactic invasive response to an applied CCL21 gradient (4 ng/ml/μm) in 3D matrices, a response that could be blocked by co neutralization of CCL21 and CCR7 (Figure 2G). Thus, tumor cell CCR7 was functional in driving a chemotactic response to CCL21.

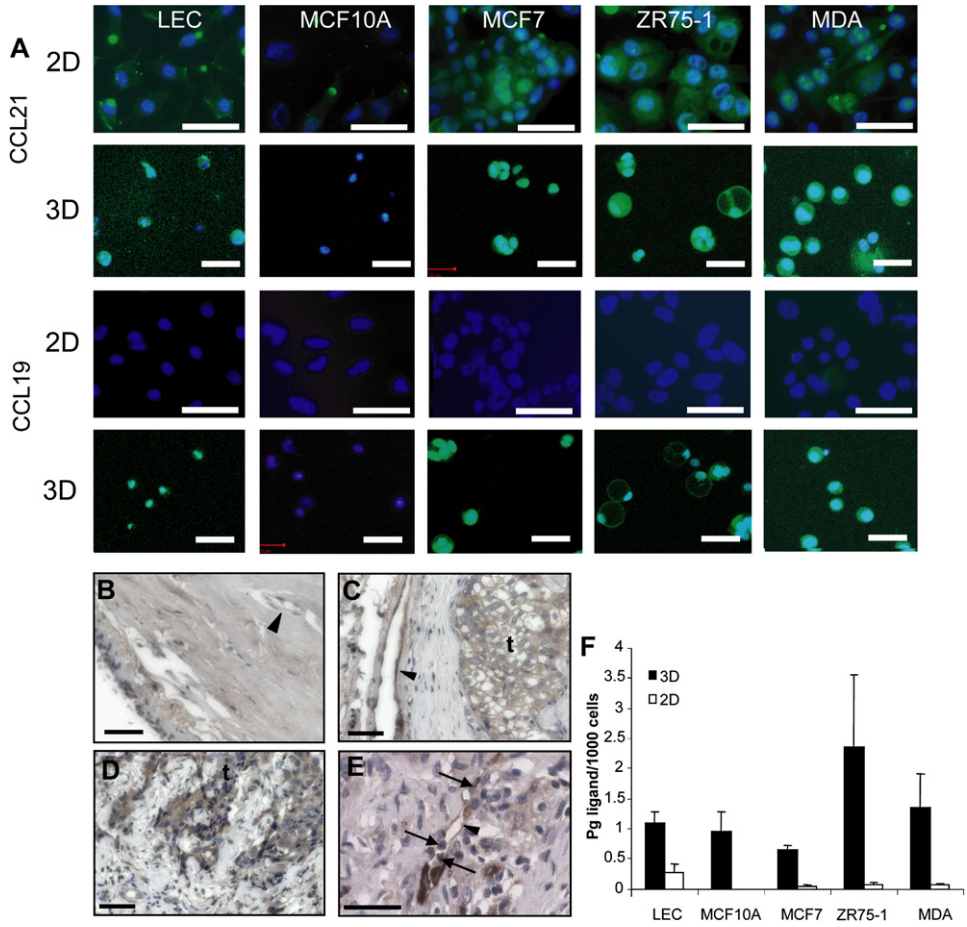

Figure 3. Autocrine Secretion of CCR7 Ligands by Tumor Cells Higher in 3D versus 2D Culture

(A) Immunostaining for CCL21 and CCL19 (green) after 24 hr culture in 2D (scale bars, 25 μm) versus a 3D Matrigel matrix (scale bars, 50 μm). No CCL19 was detected in 2D culture for any cell line, consistent with ELISA results (data not shown). Nuclei are shown in blue.

(B–E) Human tissue samples were also stained for CCL21 to confirm autocrine ligand production in vivo. (B) Very low levels of CCL21 were detected in normal breast ductal tissue. (C) CCL21 was consistently detected in carcinoma in situ (brown staining, "t"), in invasive ductal carcinoma cells (D), and also in surrounding lymphatic vessel endothelial cells (arrowheads). (E) CCL21-positive tumor cells (arrows) were observed within a similarly CCL21-positive peritumoral invasive ductal carcinoma lymphatic vessel (arrowhead). Scale bars, 50 μm.

(F) Comparison of total CCR7 ligand secreted by cells in 2D versus 3D culture by ELISA demonstrates substantially higher secretion rates of CCL21 and CCL19 in 3D culture for all cell lines tested, indicating the importance of microenvironment on chemokine signaling between tumor cells and lymphatics. Error bars represent mean ± SD.

Autocrine Secretion of CCR7 Ligands by Tumor Cells

Although it was no surprise to find CCR7 on metastatic tumor cells, as has previously been demonstrated, we also observed autocrine secretion of CCR7 ligands CCL19 and CCL21 (Figures 3A–3F). The more highly invasive cell lines (MDA-MB-435S and ZR75-1) secreted more CCR7 ligands than the MCF7 cells, MCF10A cells, or LECs. Of note, tumor cell secretion of both CCL19 and CCL21 was significantly higher in 3D than 2D culture conditions (Figures 3A and 3F), and CCL19 was not detected in 2D cultured cells (Figure 3A). In 3D, the bound protein fraction was higher than the soluble fraction (data not shown) as would be expected due to their known matrix binding properties (Patel et al., 2001). These observations emphasize the importance of the microenvironment when studying tumor cell behavior, particularly with regards to chemokine signaling as well as indicating a role for autocrine CCR7 signaling in tumor cells.

Consistent with these in vitro results, we observed CCL21 in human breast cancer tissue, with higher expression seen in DCIS and invasive carcinoma compared to normal tissue (Figures 3B and 3D). Peritumoral lymphatics were also CCL21 positive (Figure 3C, arrowhead), and CCL21-expressing tumor cells could be found within a CCL21-positive lymphatic vessel (Figure 3E), corroborating that in an in vivo setting the tumor cells secrete CCL21 as well as the lymphatics.

Paracrine Effects: CCR7-Mediated Tumor Cell Chemotaxis toward LECs

First, to determine whether tumor cells migrate toward lymphatics via CCR7 signaling as would be expected,

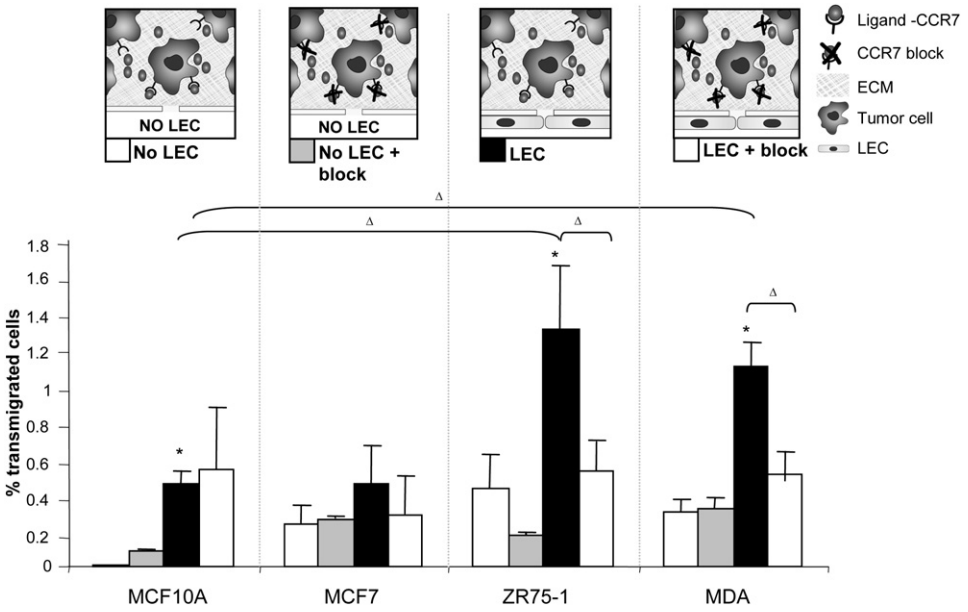

Figure 4. Tumor Cell Chemotaxis toward LECs Is CCR7 Mediated

Chemotaxis through a 3D matrix of each cell type toward LECs, with and without CCR7-blocking antibody cocktail (LEC and LEC block), as compared to basal conditions (no LEC) with or without blocking antibody (conditions illustrated in schematics). MCF10A cells, which showed little CCR7 expression, were mildly chemotactic toward LECs, although in a CCR7-independent manner. MCF7, which showed higher CCR7 expression than MCF10A but responded weakly to an imposed CCL21 gradient, also showed a small but statistically insignificant 3D chemotaxis toward LECs. Both ZR75-1 and MDA-MB-435S cells were strongly chemoattracted to LECs (*$p < 0.05$ compared with no LEC basal conditions; $^{\Delta}p < 0.05$ between other groups as indicated, and their chemotaxis was blocked with anti-CCR7 blocking). Error bars represent mean ± SD.

we used our coculture model (Figures 1B and 1C) to investigate tumor cell chemoinvasion, or chemotaxis through a 3D matrix, toward LECs under static conditions using primary human dermal LECs (Figure 1D). No LEC morphogenesis was observed in this model, nor was any LEC-induced morphogenesis of tumor cells. First, we saw that MCF10A cells weakly migrated toward LECs, and that this migration was CCR7 independent, since neutralizing antibodies against CCR7 and CCL21 did not alter migration (Figure 4). MCF7 cells were also weakly chemotactic toward LECs, but this was CCR7 dependent, since CCR7/CCL21 blocking reduced chemotaxis toward LECs to basal levels. The similarity of responses observed between these two cell types, despite their differences in chemokine secretion, can be reconciled by comparing their CCR7 expression: although MCF10A cells appear to produce higher levels of CCR7 ligand, they cannot effectively respond due to the limited CCR7 expression. In contrast, CCR7 expression is high on MCF7 cells and thus any CCR7 ligand produced by these cells can efficiently signal. The two invasive cell lines, ZR75-1 and MDA-MB-435S, both of which express high levels of CCR7 receptor and ligand, showed strong CCR7-dependent chemotaxis toward LECs. These results demonstrate that LECs chemoattract tumor cells through a 3D matrix via CCR7 signals, and that more invasive cells chemotact more strongly toward LECs than nonexpressing cells, at least for the cell lines tested here.

Autologous Chemotaxis of Tumor Cells by Interstitial Flow

To investigate the effects of IF on autologous chemotaxis of tumor cells, we introduced slow flow of 0.2 μm/s, which is within measured in vivo values (Chary and Jain, 1989; Dafni et al., 2002), through the 3D cell-Matrigel construct in the absence of LECs. Strikingly, this slow flow drove similar chemotactic responses by the tumor cells as did the LECs under static conditions (Figure 5). Flow also enhanced the migration of nontumorigenic MCF10A cells by a small but significant degree, but this enhancement was not affected by blocking CCR7 signaling (Figure 5). In contrast, the three tumor cell lines displayed marked increases in migration in the flow direction that could be inhibited by CCR7 blocking (Figure 5), indicating that the flow-enhanced migration was a CCR7-mediated chemotactic phenomenon, yet with no exogenous CCR7 ligands or LECs to signal. Furthermore, their response was correlated with invasion (at least in the cell lines tested): ZR75-1 and MDA cells displayed the strongest "autologous chemotaxis" in response to IF. These results clearly demonstrate that autologous chemotaxis toward gradients of CCR7 ligand occurred in these tumor cells under IF.

Interestingly, the migration in response to flow when CCR7 signaling was blocked was roughly equal in all four cell lines, despite their varying responses to flow. This suggested that flow had a small additional CCR7-independent effect. It is probable that this increase was primarily a consequence of directed proteolysis, as the

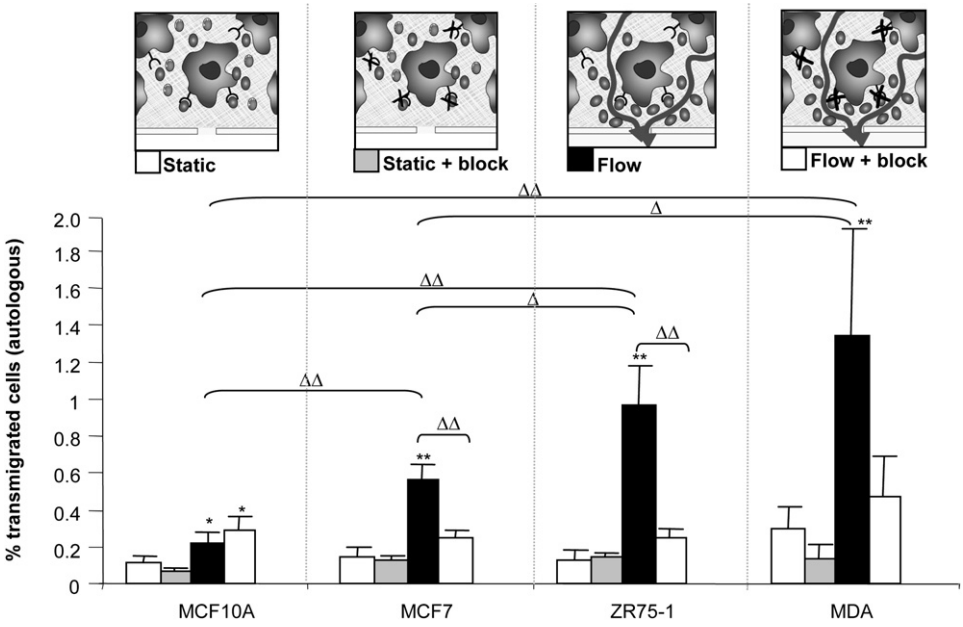

Figure 5. Autologous Tumor Cell Chemotaxis by Interstitial Flow Is CCR7 Dependent

Autologous chemotaxis of each cell type, cultured without LECs, in the direction of 0.2 μm/s interstitial flow, with and without CCR7-blocking antibody cocktail as compared to static conditions. In all cases, CCR7 blocking did not significantly affect baseline (static) migration rates. The 3D migration of MCF10A cells, which showed little CCR7 expression, doubled in the presence of flow but was unaffected by CCR7 blocking as expected. MCF7 cells, which showed higher CCR7 expression than MCF10A cells, also responded weakly to IF, but in contrast, this increase was CCR7 dependent. Migration of both ZR75-1 and MDA-MB-435S cells increased dramatically under 0.2 μm/s interstitial flow, and this increase was reversed by CCR7 blocking (*$p < 0.05$; **$p < 0.01$ compared with static conditions; $^{\Delta}p < 0.05$; $^{\Delta\Delta}p < 0.01$ between other groups as indicated). Error bars represent mean ± SD.

pan-MMP inhibitor GM6001 abolished all flow-enhanced migration (data not shown).

To more directly visualize autologous chemotaxis, we examined the localization in ZR75-1 cells of (1) the pleckstrin homology domain of the signaling molecule AKT (PHAKT) in live cells, using lentiviral transduction of the PHAKT-eGFP transgene; (2) f-actin in fixed cells; and (3) RAC in fixed cells. PHAKT, normally localized in the cytoplasm, becomes recruited to the plasma membrane as part of a receptor signaling complex that includes RAC when, following stimulation, f-actin cytoskeleton reorganization is required (e.g., during chemotaxis), indicating polarization, which alludes to subsequent cell movement (Servant et al., 2000). Using real-time fluorescence microscopy, we observed polarization responses under static, flow, and flow + CCR7 neutralization conditions. In static 3D conditions, cellular PHAKT-eGFP localization was weak and randomly directed (Figure 6A), while under IF, localization was visibly enhanced, polarizing in the general direction of flow (Figure 6B), consistent with the migration data. Significantly, when these cells were exposed to IF in the presence of blocking antibodies to CCR7 and CCL21, polarized membrane localization of PHAKT was inhibited and reflected a similar distribution of polarization directions as displayed by static cultures (Figure 6C). As a positive control, we saw biased PHAKT localization in the direction of an imposed CCL21 gradient under static conditions (Figure 6J, with a cell in 2D exposed to the same CCL21 gradient shown in Figure 6K as a comparison).

It is well established that small GTPases regulate cytoskeleton dynamics in response to migratory stimuli; in particular, Rho GTPases such as RAC mediate f-actin polymerization at the polarizing cell's leading edge (as reviewed in Charest and Firtel, 2007; Fukata et al., 2003). Consistent with the PHAKT data, we saw that flow induced preferential actin localization at the leading edge of the cell (Figure 6E), which was not repeated in either "static" (Figure 6D) or "flow + block" (Figure 6F) conditions. Polarized RAC expression was also observed under the influence of IF (Figure 6H) but not under flow + block conditions (Figure 6I). Thus, IF mediated not only preferential migration, but also cell polarization that was dependent on autocrine CCR7 signaling.

To quantify this polarization effect of IF, each cell was scored (Figure 6L) and classified as (1) nonpolarized, (2) polarized with flow direction (region I, 0°–60°), (3) polarized orthogonal to the direction of flow (region II, 60°–120°), or (4) polarized against flow direction (region III, 120°–180°). In all cases—static, flow, flow + block, and static with an applied CCL21 gradient—more than half of all cells did not show any polarization. In those cells that did polarize, no directional biases were seen in static conditions, but cells under flow displayed a 4-fold increase in directional bias toward flow that was abolished when CCR7 signals were blocked (Figure 6M). Hence, under static conditions,

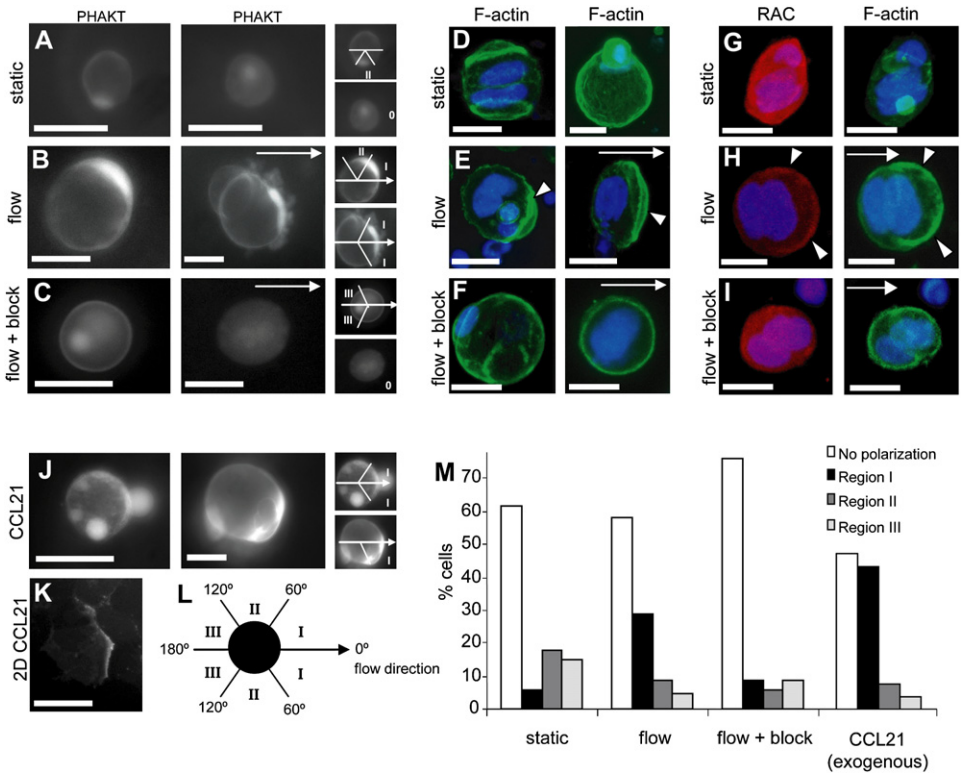

Figure 6. Polarization of Cells in Response to Biophysical and Biochemical Stimuli

(A–C) PHAKT-eGFP localization and polarization within ZR75-1 cells in two representative cells (left and right panels) from 3D static gels (A), 3D gels under interstitial flow (B), and 3D gels under interstitial flow with CCR7-blocking antibody cocktail (C). Live microscopy demonstrated that flow was able to induce directional polarization that was CCR7 dependent; inhibition of CCR7 signaling prevented polarization responses. Arrows represent flow direction. Insets indicate examples of quantification for representative cells. (D–F) Staining of fixed samples with phalloidin in two representative cells (left and right) demonstrates directional reorganization and membrane localization (arrowheads) of the actin cytoskeleton in a flow-dependent (E) and CCR7-dependent (F) manner. No reorganization was observed in static conditions (D). Arrows represent flow direction. (G and I) Colabeling of fixed cells following live experiments reveals that membrane localization of the signaling molecule RAC (left panel) coincident with F-actin (right panel) could only be detected in cells exposed to IF ([H], arrowheads). This was not apparent in static (G) or flow + block (I) situations. Arrow denotes flow direction. (J and K) Live-imaged PHAKT-eGFP localization and polarization within ZR75-1 cells in two representative images of 3D gels with an exogenous 1% transcellular CCL21 protein gradient (J), and the same CCL21 gradient in 2D culture (K); for cells in static conditions, one arbitrary direction was fixed as the reference direction. Insets indicate examples of quantification for representative cells. Scale bars, 50 μm in (A)–(C), (J), and (K), 25 μm in (D)–(I). (L) Criteria for quantifying polarization responses of cells. Each cell was scored according to its orientation relative to the direction of flow or imposed CCL21 gradient and assigned as not polarized or polarized in one of three regions (directed parallel [I], orthogonal [II], or opposite [III] to the direction of flow) as shown. (M) Summary of cell polarization in response to flow. In all cases, roughly half or more of analyzed cells were not polarized. Among those cells that did polarize, PHAKT-eGFP localization was directionally unbiased in static and flow + block conditions, in contrast to conditions of flow and exogenous CCL21 gradient, where cells preferentially polarized with rather than against the direction of flow or exogenous chemotactic gradient.

or when signaling was prevented, there were effectively no biasing factors and cells polarized randomly or not at all. In contrast, when exposed to IF, cells polarized in the direction of flow similarly as those exposed to an applied CCL21 gradient of 5.5 μg/ml/mm. This further supported the notion of IF-induced, CCR7-dependent autologous chemotaxis.

Combined Effects of Flow and LECs Lead to Amplified Response

Finally, using the most invasive cell line, MDA-MB-435S, we examined the combined response of tumor cells to LECs and IF (Figure 1A), as would occur in vivo. As expected, the two effects combined to drive even stronger chemotaxis in the direction of LECs than did either factor alone (Figure 7A). Combined, flow-enhanced migration of tumor cells toward LECs was roughly three times that of their migration toward either cue alone. When CCR7 signaling was blocked, the percent migration was not significantly different than either that seen with flow alone with blocking, or that with LECs alone with blocking, indicating that the combined synergistic effect was also CCR7 mediated.

Computational Modeling of the Tumor-Lymphatic Microenvironment

To explain the autologous chemotactic effects observed, we hypothesized that IF could bias the distribution of

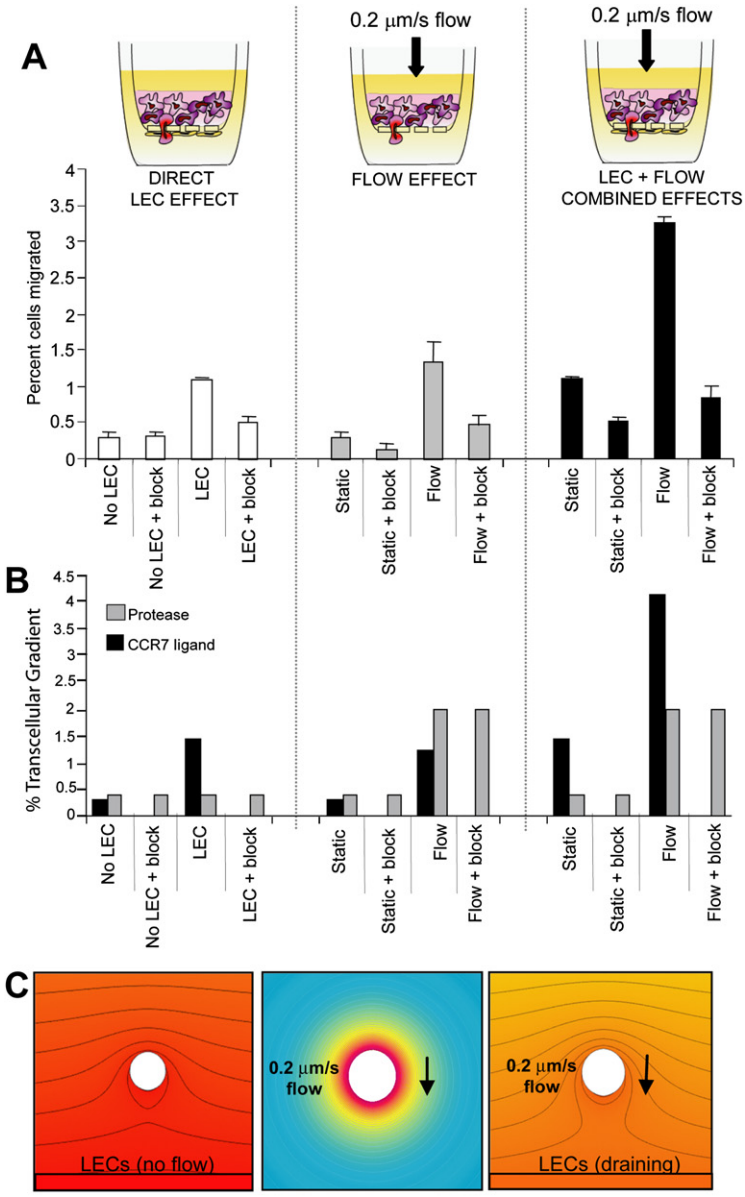

Figure 7. Combined Effects and Computational Modeling

(A) Summary of in vitro migration experiments comparing the individual and combined effects of LECs, interstitial flow, and CCR7 blocking on transmembrane migration of MDA-MB-435S cells demonstrate that both autocrine and paracrine signaling are CCR7 dependent, and that the combined effects of flow and LECs are stronger than either effect alone.

(B) Computed transcellular chemokine and protease gradients perceived by cells are consistent with in vitro migration trends: first, both LECs (in static conditions) and interstitial flow (in LEC-free conditions) impose similar CCR7 ligand gradients, just as they produced similar migratory responses in tumor cells. Second, the combined gradient is nearly three times larger than that for LECs or interstitial flow alone. Gray bars represent transcellular protease gradients that may potentially cause a secondary effect of directed proteolysis that could explain above-baseline migration levels that persist in flow conditions even with the use of blocking antibodies.

(C) Graphical representation of CCL21/19 gradients around a tumor cell embedded in 3D matrix corresponding to (left to right) static culture with LECs, interstitial flow without LECs, and interstitial flow with LECs. Red-blue color gradient indicates maximal-to-zero concentration, and arrow indicates direction of flow.

(D) Numerical results tabulated for direct comparison. Protease concentration differences are normalized against the value for the static case.

Error bars represent mean ± SD.

D

	Transcellular Chemokine Gradient (%)		Migration (%)		Dimensionless Trancellular Protease Gradient	
Condition	Static	Flow	Static	Flow	Static	Flow
No LECs	0.3*	1.2	0.3	1.3	1*	4.7
No LECs + Block	0.0	0.0	0.3	0.4	1*	4.7
LECs	1.4	4.1	1.1	3.3	1*	4.7
LECs + Block	0.0	0.0	0.5	0.8	1*	4.7

*A small amount of asymmetry persists even in static conditions due to the geometry of the transwell experiment (i.e. much more media above the gel layer than below)

CCL21 and CCL19 released by the tumor cell and, together with similar biasing of cell-released proteases that could further liberate bound chemokines from the matrix, create pericellular gradients of autocrine CCR7 ligands that increase in the downstream direction to drive chemotaxis. This was based on recent findings that slow flow could synergize with matrix-bound vascular endothelial growth factor (VEGF) to drive capillary morphogenesis in vitro (Helm et al., 2005), and on recent computational modeling describing how such gradients might be formed (Fleury et al., 2006). It is important to note that, under such conditions, diffusion still dominates the overall transport problem—the Peclet number, which describes the relative contribution of convection compared to diffusion in the overall transport, is only 0.02—but the contribution of convective transport is sufficient to skew the diffusion gradient downstream and actually create a difference in concentration between upstream and downstream sides of the cell. In other words, while diffusion determines the overall magnitude of the chemokine gradient away from the cell, convection changes its shape, and thus gradient, relative to the cell.

We modeled the specific case of CCR7 ligands (CCL19 and 21) secreted by a cell into the pericellular matrix under 0.2 μm/s flow. First, the ligands were assumed to be secreted uniformly from a 20 μm cell at constant flux and transported away from the cell by diffusion and convection, and CCL21 was also subject to matrix binding according to its equilibrium-binding kinetics with heparan sulfate (Uchimura et al., 2006). The same cell was also considered to secrete matrix-degrading enzymes (MMPs, sulfatases, etc.) that were capable of further liberating ECM-bound CCL21, so that the final soluble CCL21/19 profile was a combination of cell-secreted and ECM-released ligands. Only this soluble fraction of ligand was assumed to bind CCR7. This differs from previously presented cases, where ligand was initially present uniformly bound to the matrix, or where ligand was secreted in a pro-form and only active upon protease cleavage (Fleury et al., 2006; Helm et al., 2005). We modeled all experimental cases, comparing autocrine, paracrine, and combined signaling under conditions of static versus flow, and with and without CCR7 blocking.

Chemotaxis in 3D is the result of a combination of signaling inputs to the cell, matrix compliance, and active cellular response such as the engagement of cell motility machinery. The computational model addressed only the signaling input to the cell with the implicit assumption that the overall chemotactic response would be proportional to this stimulus (Janetopoulos et al., 2004). The predicted chemokine gradients were indeed qualitatively consistent with our experimental migration results. First, we predicted that paracrine effects of LEC-secreted CCL21/19 (under static conditions) induced a transcellular ligand gradient of 1.4% across the tumor cell surface (Figure 7B). During the transient portion of the gradient formation, this value varies with time and location through the 500 μm thick matrix; we chose to model a reference cell 150 μm from the bottom boundary of the gel, which is within the limits of where the cells that transmigrate in 15 hr would be expected to be located within the gel originally.

We then modeled autocrine effects (no LECs) and saw that interstitial flow of 0.2 μm/s can bias the transcellular gradient of both CCL21/19 and cell-secreted proteases in the direction of flow (Figure 7B). These data correspond qualitatively with the in vitro results (Figures 7A and 7D). Specifically, we found that the calculated CCL21/19 transcellular gradient, which would act as the chemotactic stimulus for a cell, was similar between a tumor cell alone under flow (1.2%) and the static case when LECs are present (1.4%), which was consistent with the experimental data demonstrating that these two conditions had each induced similar migration responses (1.3% and 1.1% flow alone and LECs alone, respectively).

When both autocrine and paracrine effects were combined with flow effects, the transcellular gradient was increased approximately 3-fold, which was consistent with the experimental results showing that the percentage of transmigrated cells was also roughly tripled compared to either condition alone. While we hypothesize that migration is principally driven by biased CCL21 gradients, a secondary mechanism may also be present: proteases secreted by tumor cells are also subject to the biasing effects of interstitial flow (Figures 7B and 7D), which could lead to increased migration in the direction of flow due to directed proteolysis. While CCR7 blocking should abolish the chemotactic mechanism, it should not affect directed proteolysis (Figure 7B). Consistent with this notion, in vitro migration experiments show that, while CCR7 blocking inhibits flow-enhanced migration, there still remain some residual enhancement of migration (although not statistically significant in any cell type) compared to that in static controls (Figure 7A).

Thus, our experimental results demonstrate that (1) slow IF can induce autologous chemotaxis of tumor cells in the direction of flow; (2) slow IF steepens the gradient of CCR7 ligand secreted by LECs to enhance paracrine chemotaxis of tumor cells toward LECs; and (3) when IF is directed toward CCL21-secreting LECs, i.e., when a lymphatic is functional and draining fluid, the combination of effects leads to a greatly enhanced chemotactic transcellular gradient to further drive tumor cells toward the lymphatic.

DISCUSSION

This study highlights the importance and relevance of the biophysical microenvironment to lymphatic metastasis and introduces a mechanism that we term autologous chemotaxis whereby autocrine chemokine secretion directs tumor cells to chemotact in the direction of flow, i.e., toward draining lymphatics. It provides mechanistic insight into why CCR7 expression correlates with lymph node metastasis in human cancers (Gunther et al., 2005; Heresi et al., 2005; Shields et al., 2007; Takeuchi et al., 2004; Wang et al., 2005; Wiley et al., 2001) and introduces the concept that tumor invasiveness toward draining

lymphatics, at least in vitro, is correlated with autocrine secretion of CCR7 *ligands*. Furthermore, when the tumor cell comes in close proximity to a lymphatic, which can also secrete CCR7 ligand, the tumor-derived CCL21/19 gradient can add to the lymphatic-secreted CCL21 to further augment the chemotactic response of tumor cells toward functional draining lymphatics. Interestingly, while IF decreases the transport distance of CCL21 secreted by the lymphatics, it actually *increases* the transcellular gradient across a nearby tumor cell (within its broadcast distance), since the concentration gradient becomes steeper. This is important because chemotacting cells respond to a concentration difference rather than an absolute amount (Zigmond, 1977; Janetopoulos et al., 2004).

Because IF is always directed from the tumor toward the lymphatic, and because chemokine signaling appears to play a critical role in lymphatic homing of tumor cells, an experimental model system to study tumor-lymphatic interactions should both include appropriate levels of interstitial flow and allow for chemokine signaling to occur. Experimental models of tumor-lymphatic interactions have been mostly limited to human tumor xenografts in mice, where relative migration is difficult to assess, and where chemokine signaling varies due to compromised immune systems and potential incompatibilities between some rodent and human cytokines. Standard in vitro chemotaxis assays often do not include biophysical factors, like ECM and IF, which could strongly affect transport and distribution of secreted chemokines and thus relevant cell-cell signaling events. Tissue-engineered 3D models have advantages over both in vivo and traditional in vitro models for examining interactions between human cells in an environment that recapitulates some biophysical features of the natural in vivo situation (Griffith and Swartz, 2006).

Using a 3D in vitro coculture model, we demonstrate how biophysical factors of the tumor-lymphatic microenvironment favor tumor cell migration toward functional lymphatics. We saw that melanoma and breast tumor cells secrete CCL21 and CCL19, and that they do so to a much higher degree when maintained within a 3D matrix than in 2D. Furthermore, these cells are responsive to CCR7 ligand and can chemotact up an imposed CCL21 gradient as well as toward LECs in a CCR7-dependent manner. Strikingly, physiological levels of IF significantly enhanced tumor migration in the direction of flow, with and without LECs. These responses could be reversed by blocking CCR7 signals, clearly illustrating that flow-enhanced migration is a phenomenon of CCR7-dependent chemotaxis. Computational simulation of CCL21/19 transport under this flow estimated a transcellular CCL21/19 gradient to be 1.2% without LECs and 4.1% with LECs. Although the limits for tumor cell sensing of CCL21/19 gradients are not known, it has been shown that neutrophils can directionally sense as little as 1% differences in transcellular concentration of chemoattractant (Zigmond, 1977), and similarly, small morphogen gradients are known to act as positional cues for cells in many developing tissues (Ashe and Briscoe, 2006; Yucel and Small, 2006). Furthermore, we demonstrated, using the PHAKT-eGFP cell polarization marker as well as by staining for f-actin and RAC, that such imposed biophysical cues alone could initiate cellular signaling events needed for actin reorganization and cell polarization. Thus, it is highly probable that small transcellular chemokine gradients formed by flow are responsible for stimulating chemotaxis of tumor cells in the direction of flow.

In conclusion, we have demonstrated the importance of the tumor-ECM-lymphatic microenvironment for lymphatic metastasis and identified a mechanism for tumor cell homing to lymphatics that is consistent with human cancer data correlating CCR7 expression with lymph node metastasis. In addition to introducing autologous chemotaxis, this is, to our knowledge, the first demonstration that tumor cells can respond to autocrine CCR7 ligands, and also that physiological levels of IF can enhance tumor cell migration in the direction of flow. These results help elucidate fundamental mechanisms of tumor cell invasion of lymphatics and may also be relevant to understanding how leukocytes home to lymphatics.

EXPERIMENTAL PROCEDURES

Antibodies, Flow Cytometry, and Immunofluorescence

Neutralizing antibodies against human CCL21 (AF366) and CCR7 (MAB197) were purchased from R&D Systems (Minneapolis, MN) and used at 4 μg/ml and 5 μg/ml, respectively. Antibodies against human podoplanin (gp36; 10 μg/ml, Cell Sciences, Inc., Canton, MA), CD31 (10 μg/ml, BD Pharmingen, San Diego, CA), LYVE-1 (15 μg/ml, RELIATech, Braunschweig, Germany), and Prox1 (5 μg/ml, RELIATech) were used with mouse IgG as a control (10 μg/ml, Sigma). Alexa Fluor 488-labeled IgGs (Molecular Probes, Carlsbad, CA) were used for detection, and DAPI (Vector Laboratories, Burlingame, CA) was used for counterstaining nuclei. Cytoskeleton polarization machinery was stained for RAC (10 μg/ml, AbCAM) and f-actin (AF488 Phalloidin, Molecular Probes). Immunostaining was performed for CCL21 (15 μg/ml, AF366), CCL19 (8 μg/ml, AF361), and CCR7 (25 μg/ml, MAB197) (all R&D Systems).

Sections from archived malignant human breast tissue samples (kind gift from Dr. Cathrin Brisken, obtained under the authority of the Ethics Committee of the Centre Hospitalier Universitaire Vaudois with patient consent) and normal breast tissue (ab4324, Abcam) were subjected to standard immunohistochemistry for CCR7 (8 μg/ml) and CCL21 (8 μg/ml) and counterstained with hematoxylin.

Cell Culture

MCF10A, MCF7, ZR75-1, and MDA-MB-435S cells (all from ATCC/LGC Promochem, Middlesex, UK) were maintained in 1:1 DMEM:F12 Hams (with 0.01 mg/ml bovine insulin, 0.5 μg/ml hydrocortisone, 20 ng/ml EGF, 5% FBS, and 1% penicillin-streptomycin), α-MEM (with 2 mM L-glutamine, 1 mM sodium pyruvate, 0.01 mg/ml bovine insulin, 10% FBS, and 1% penicillin-streptomycin), RPMI 1640 (with 2.5 g/l D-glucose, 1 mM sodium pyruvate, 10 mM HEPES, 10% FBS, and 1% penicillin-streptomycin), and DMEM with 10% FBS, respectively. Human dermal LECs were isolated from neonatal foreskin and cultured as previously described (Podgrabinska et al., 2002) and immunostained for typical LEC markers (Figure 1D).

Reverse Transcriptase PCR

Total RNA was isolated with RNAqueous extraction kit (cat number 1912, Ambion, Austin, TX) according to the manufacturer's guidelines. CCR7 fragments were amplified using forward primer

5′-GACCGATACCTACCTGCTCAACC-3′ and reverse primer 3′-GCTC ACTGCTGCTCCTCTGG-5′ to yield a product of 341 bp. A human P0 control (data not shown) was included using forward primer 5′-GCCA CGCTGCTGAACATGCTCAAC-3′ and reverse primer 3′-CCGACTCC TCCGACTCTTCCTTGG-5′ to yield a product of 409 bp.

Static Migration Assay

Experiments were performed with 12 mm diameter, 8 μm pore cell culture inserts (Millipore, Billerica, MA) in a modified Boyden chamber assay. For chemotactic gradient studies, 50,000 tumor cells were seeded in 150 μl (1 mm thick) Matrigel (4.65 mg/ml, BD Biosciences, San Jose, CA). Basal medium was placed in the top chamber, while the bottom contained basal medium either alone, with 350 ng/ml CCL21 protein, or with both CCL21 protein and a cocktail of anti-CCR7 and anti-CCL21 blocking antibodies (in the latter case, antibodies were also included in the top chamber). After 15 hr in a 37°C/5% CO_2 incubator, Matrigel containing nonmigrated cells was removed and the inserts were fixed in chilled methanol. The membrane was removed and mounted with Vectashield containing DAPI (Vector), and the number of migrated cells was counted.

Coculture Migration Assay

For assessing chemotaxis of tumor cells toward LECs, a coculture assay, modified from the above setup, was used. LECs were seeded onto the collagen-coated underside of the chamber at 100,000 cells/well and cultured to confluence (3 days). The migration assay was then prepared as described above but modified to incorporate 50,000 tumor cells seeded within 50 μl Matrigel.

Migration under Flow

The above setup was modified to examine the effects of physiological flow on tumor cell migration, either with or without LECs on the underside of the chamber as described. After the Matrigel was cast and allowed to set, a pressure head of 1 cm water was established that led to an average velocity of 0.2 μm/s through the cell/gel compartment (flow rate determined in separate experiments both by direct measurements and using measured permeability; data not shown). Migration in the presence of basal media, alone or with anti-CCR7 and anti-CCL21 blocking antibodies, and with or without flow, was assessed.

Western Blot Analysis

CCR7 expression was analyzed by Western blot using 0.5 μg/ml mouse anti-CCR7 (R&D Systems), HRP-conjugated goat anti-mouse IgG (BioRad), and a Western Pico ECL substrate kit (Pierce, Rockford, IL). Sample loads were normalized to cell number in three separate experiments.

ELISA

CCL19 and CCL21 protein secretion was quantified using ELISA kits (R&D) from cells maintained in both 2D and 3D culture conditions in basal media. For 2D samples, conditioned media were collected after 24 hr culture. 3D samples were analyzed following culture of 450,000 cells per well (in 24-well plates) within 300 μl of Growth Factor Reduced Matrigel in basal media for 24 hr. To account for matrix-bound ligands, three compartments were analyzed by ELISA: medium, matrix protein (by digestion with Cell Recovery Solution [BD Biosciences, San Jose, CA]), and cells (by lysis using standard RIPA buffer protocols [Sigma]).

Computation of Extracellular CCL21 Distribution

Pericellular CCL21/19 gradients were computed using a 3D model according to the following:

$$\frac{dC_i}{dt} + v \cdot \nabla C_i = D_i \nabla^2 C_i + R_i$$

where C_i is concentration of species i, t is time, v is velocity vector, D_i is the diffusion coefficient, and R_i is the rate of reaction (disappearance due to matrix binding or appearance due to unbinding or proteolytic release from the matrix). The cell was modeled as a 20 μm diameter sphere embedded 150 μm from the bottom surface of a 500 μm thick porous ECM (Matrigel) with 3 mm of medium atop the matrix. In simulations involving LECs, the cells were modeled on the bottom of the ECM layer with a cell density obtained using micrographs of in vitro preparations. The Brinkman equation was used to calculate the velocity profile through the porous ECM around the cell using a value for permeability $K = 10^{-12}$ cm^2 (calculated from our experimental data) and average v = 0.2 μm/s. Four species i were modeled: P, the cell-released protease; *CCL21*, the cell-released CCL21; *CCL19*, the cell-released CCL19; and *HS-CCL21*, the matrix-bound CCL21. Constant flux boundary conditions were assumed for both P and CCL21/19 at cell surfaces, with CCL21/19 fluxes measured experimentally (Figure 3), along with zero flux inlet boundary conditions. The diffusion coefficients were assumed to be 140 μm^2/s for *CCL21/19* and 80 μm^2/s for P (Fleury et al., 2006). The modeled species were subjected to the following binding and release kinetics:

$$CCL21 + HS \underset{koff}{\overset{kon}{\leftrightarrow}} HS - CCL21$$

$$HS - CCL21 + P \overset{krel}{\rightarrow} CCL21 + HS + P$$

where *HS* = heparin sulfate binding sites; *HS-CCL21* = matrix-bound CCL21; and k_{on}, k_{off}, and k_{rel} are rate constants for the reactions shown. k_{on} and k_{off} were assumed to be 9.3 × 10^4 M^{-1}s^{-1} and 1.2 × 10^{-4}s^{-1}, respectively, based on our own measurements (data not shown), and k_{rel} was assumed to be 1 × 10^5 M^{-1}s^{-1}. (This value was chosen arbitrarily to make the release term on the same order of magnitude as the "on" rate, but parametric variation of k_{rel} revealed that, while its value affected absolute CCL21 concentrations, it had no effect on the percent transcellular gradients calculated.) *HS* was calculated to be 1.2 μM assuming 2% proteoglycan (perlecan) content in Matrigel and 12 binding sites per perlecan molecule.

The corresponding rate equations were as follows:

$$R_{CCL21} = -k_{on} C_{CCL21} C_{HS} + k_{off} C_{HS-CCL21} + k_{rel} C_{HS-CCL21} C_P$$

$$R_{HS-CCL21} = k_{on} C_{CCL21} C_{HS} - k_{off} C_{HS-CCL21} - k_{rel} C_{HS-CCL21} C_P = -R_{CCL21}$$

where R refers to the overall rate of production and C refers to the concentration of each of the components defined above. C_{HS} was considered to be much larger than C_{CCL} based on the calculated number of binding sites in the Matrigel relative to the total CCR7 ligand concentration (Figure 3) and therefore was treated as a constant. CCL19 was assumed not to interact with the matrix and was therefore not subject to a reaction term.

Mass balances for free ligand, bound ligand, and protease were solved simultaneously in a transient analysis to estimate the combined CCR7 ligand gradients that would be established after 50,000 s, matching the experimental time frame. The calculations were performed using COMSOL Multiphysics modeling software (Berne, Switzerland) on a personal computer.

PHAKT-eGFP Polarization Assay

The fluorescent probe used to determine spatial distribution of intermediate intracellular signals between activation of chemotactic receptors and actin polymerization, the PHAKT-eGFP construct (Servant et al., 2000), was a kind gift from Tamas Balla. A cassette containing the PHAKT-eGFP, an EcoRI-HincII fragment, was blunt-end ligated into the lentivirus backbone pRRLsincPPT-hPGK-mcs-WPRE (a kind gift from Didier Trono) and expanded in competent *E. coli*. Clone DNAs from antibiotic-resistant colonies were purified and analyzed for the correct recombination event. Lentiviral vectors were produced via transfection of HEK293T cells with the PHAKT-eGFP transfer construct, pCMVR8.74 packaging plasmid, and pMD2.G envelope

plasmid in the ratio 3:2:1. Media were collected after 24 and 36 hr, and virus was concentrated by ultracentrifugation in 20% saccarose solution. ZR75-1 cells were infected with the lentivirus in 24-well plates and checked for stable expression of PHAKT-eGFP.

PHAKT-eGFP-ZR75-1 cells were seeded at 10^6 cells/ml within a matrix (3:1 collagen:Matrigel) and placed within a radial flow chamber as described (Ng et al., 2005). Slow IF, via a constant pressure head (leading to an average flow velocity of ~0.2 μm/s near the outer edge of the chamber, where images were taken) was applied to the system for 7 hr (maintained at 37°C/5% CO_2 on the microscope stage), during which time live cells were visualized and photographed on a Zeiss fluorescence microscope (Axiovert 200M). Gels were then fixed and stained for cytoskeleton machinery proteins (as described earlier) and visualized on a Zeiss LSM Meta 500 inverted confocal microscope.

For cells exposed to an exogenous CCL21 gradient in 2D or 3D, PHAKT-eGFP-ZR75-1 cells were seeded into an IBIDI μVI culture slide (Ibidi, Munich, Germany) either in basal medium or in Matrigel and allowed to establish overnight. CCL21 (350 ng/ml) was added to the inlet, and basal medium was added to the outlet, creating a 1 cm distance over which a gradient could form. Cells were maintained in this gradient for 20 min or 6 hr (2D and 3D, respectively), and then cells within 200 μm of the CCL21 depot were visualized with a Zeiss fluorescence microscope.

Statistical Analyses

To test for statistical significance between experimental groups, Kruskal-Wallis and Mann-Whitney U tests were performed. Statistical significance was assumed where $p < 0.05$. All bar graphs show mean ± SD.

ACKNOWLEDGMENTS

The authors are grateful to Olga Sazonova, Didier Foretay, Veronique Borel, and Thierry Laroche for technical assistance; Mihaela Skobe and Simona Podgrabinska for help with LEC isolation; Isabelle Barde and Didier Trono for assistance with lentiviral production; Cathrin Brisken for human tissue sections; and Tamas Balla for the generous gift of the PHAKT-eGFP construct. This work was funded by the U.S. DoD (BC046063), the NIH (RO1 HL075217-01), and the Swiss National Science Foundation (107602).

Received: February 19, 2006
Revised: March 20, 2007
Accepted: April 26, 2007
Published: June 11, 2007

REFERENCES

Arya, M., Patel, H.R., McGurk, C., Tatoud, R., Klocker, H., Masters, J., and Williamson, M. (2004). The importance of the CXCL12-CXCR4 chemokine ligand-receptor interaction in prostate cancer metastasis. J. Exp. Ther. Oncol. *4*, 291–303.

Ashe, H.L., and Briscoe, J. (2006). The interpretation of morphogen gradients. Development *133*, 385–394.

Cabioglu, N., Yazici, M.S., Arun, B., Broglio, K.R., Hortobagyi, G.N., Price, J.E., and Sahin, A. (2005). CCR7 and CXCR4 as novel biomarkers predicting axillary lymph node metastasis in T1 breast cancer. Clin. Cancer Res. *11*, 5686–5693.

Cailleau, R., Olive, M., and Cruciger, Q.V. (1978). Long-term human breast carcinoma cell lines of metastatic origin: Preliminary characterization. In Vitro *14*, 911–915.

Carmeliet, P. (2003). Angiogenesis in health and disease. Nat. Med. *9*, 653–660.

Chambers, A.F., Groom, A.C., and MacDonald, I.C. (2002). Dissemination and growth of cancer cells in metastatic sites. Nat. Rev. Cancer *2*, 563–572.

Charest, P.G., and Firtel, R.A. (2007). Big roles for small GTPases in the control of directed cell movement. Biochem. J. *401*, 377–390.

Chary, S.R., and Jain, R.K. (1989). Direct measurement of interstitial convection and diffusion of albumin in normal and neoplastic tissues by fluorescence photobleaching. Proc. Natl. Acad. Sci. USA *86*, 5385–5389.

Clarijs, R., Schalkwijk, L., Ruiter, D.J., and de Waal, R.M. (2001). Lack of lymphangiogenesis despite coexpression of VEGF-C and its receptor Flt-4 in uveal melanoma. Invest. Ophthalmol. Vis. Sci. *42*, 1422–1428.

Dafni, H., Israely, T., Bhujwalla, Z.M., Benjamin, L.E., and Neeman, M. (2002). Overexpression of vascular endothelial growth factor 165 drives peritumor interstitial convection and induces lymphatic drain: Magnetic resonance imaging, confocal microscopy, and histological tracking of triple-labeled albumin. Cancer Res. *62*, 6731–6739.

Darash-Yahana, M., Pikarsky, E., Abramovitch, R., Zeira, E., Pal, B., Karplus, R., Beider, K., Avniel, S., Kasem, S., Galun, E., and Peled, A. (2004). Role of high expression levels of CXCR4 in tumor growth, vascularization, and metastasis. FASEB J. *18*, 1240–1242.

Debes, G.F., Arnold, C.N., Young, A.J., Krautwald, S., Lipp, M., Hay, J.B., and Butcher, E.C. (2005). Chemokine receptor CCR7 required for T lymphocyte exit from peripheral tissues. Nat. Immunol. *6*, 889–894.

Ding, Y., Shimada, Y., Maeda, M., Kawabe, A., Kaganoi, J., Komoto, I., Hashimoto, Y., Miyake, M., Hashida, H., and Imamura, M. (2003). Association of CC chemokine receptor 7 with lymph node metastasis of esophageal squamous cell carcinoma. Clin. Cancer Res. *9*, 3406–3412.

Engel, L.W., Young, N.A., Tralka, T.S., Lippman, M.E., O'Brien, S.J., and Joyce, M.J. (1978). Establishment and characterization of three new continuous cell lines derived from human breast carcinomas. Cancer Res. *38*, 3352–3364.

Fleury, M.E., Boardman, K.C., and Swartz, M.A. (2006). Autologous morphogen gradients by subtle interstitial flow and matrix interactions. Biophys. J. *91*, 113–121.

Forster, R., Schubel, A., Breitfeld, D., Kremmer, E., Renner-Muller, I., Wolf, E., and Lipp, M. (1999). CCR7 coordinates the primary immune response by establishing functional microenvironments in secondary lymphoid organs. Cell *99*, 23–33.

Fukata, M., Nakagawa, M., and Kaibuchi, K. (2003). Roles of Rho-family GTPases in cell polarisation and directional migration. Curr. Opin. Cell Biol. *15*, 590–597.

Griffith, L., and Swartz, M. (2006). Capturing complex 3D tissue physiology *in vitro*. Nat. Rev. Mol. Cell Biol., in press.

Gunn, M.D., Tangemann, K., Tam, C., Cyster, J.G., Rosen, S.D., and Williams, L.T. (1998). A chemokine expressed in lymphoid high endothelial venules promotes the adhesion and chemotaxis of naive T lymphocytes. Proc. Natl. Acad. Sci. USA *95*, 258–263.

Gunther, K., Leier, J., Henning, G., Dimmler, A., Weissbach, R., Hohenberger, W., and Forster, R. (2005). Prediction of lymph node metastasis in colorectal carcinoma by expression of chemokine receptor CCR7. Int. J. Cancer *116*, 726–733.

He, Y., Rajantie, I., Pajusola, K., Jeltsch, M., Holopainen, T., Yla-Herttuala, S., Harding, T., Jooss, K., Takahashi, T., and Alitalo, K. (2005). Vascular endothelial cell growth factor receptor 3-mediated activation of lymphatic endothelium is crucial for tumor cell entry and spread via lymphatic vessels. Cancer Res. *65*, 4739–4746.

Helm, C.L., Fleury, M.E., Zisch, A.H., Boschetti, F., and Swartz, M.A. (2005). Synergy between interstitial flow and VEGF directs capillary morphogenesis in vitro through a gradient amplification mechanism. Proc. Natl. Acad. Sci. USA *102*, 15779–15784.

Heresi, G.A., Wang, J., Taichman, R., Chirinos, J.A., Regalado, J.J., Lichtstein, D.M., and Rosenblatt, J.D. (2005). Expression of the chemokine receptor CCR7 in prostate cancer presenting with

generalized lymphadenopathy: Report of a case, review of the literature, and analysis of chemokine receptor expression. Urol. Oncol. *23*, 261–267.

Jain, R.K. (2003). Molecular regulation of vessel maturation. Nat. Med. *9*, 685–693.

Jain, R.K. (2005). Normalization of tumor vasculature: An emerging concept in antiangiogenic therapy. Science *307*, 58–62.

Janetopoulos, C., Ma, L., Devreotes, P.N., and Iglesias, P.A. (2004). Chemoattractant-induced phosphatidylinositol 3,4,5-trisphosphate accumulation is spatially amplified and adapts, independent of the actin cytoskeleton. Proc. Natl. Acad. Sci. USA *101*, 8951–8956.

Kleinman, H.K., and Martin, G.R. (2005). Matrigel: Basement membrane matrix with biological activity. Semin. Cancer Biol. *15*, 378–386.

Mandriota, S.J., Jussila, L., Jeltsch, M., Compagni, A., Baetens, D., Prevo, R., Banerji, S., Huarte, J., Montesano, R., Jackson, D.G., et al. (2001). Vascular endothelial growth factor-C-mediated lymphangiogenesis promotes tumour metastasis. EMBO J. *20*, 672–682.

Mashino, K., Sadanaga, N., Yamaguchi, H., Tanaka, F., Ohta, M., Shibuta, K., Inoue, H., and Mori, M. (2002). Expression of chemokine receptor CCR7 is associated with lymph node metastasis of gastric carcinoma. Cancer Res. *62*, 2937–2941.

Muller, A., Homey, B., Soto, H., Ge, N., Catron, D., Buchanan, M.E., McClanahan, T., Murphy, E., Yuan, W., Wagner, S.N., et al. (2001). Involvement of chemokine receptors in breast cancer metastasis. Nature *410*, 50–56.

Nathanson, S.D. (2003). Insights into the mechanisms of lymph node metastasis. Cancer *98*, 413–423.

Ng, C.P., Hinz, B., and Swartz, M.A. (2005). Interstitial fluid flow induces myofibroblast differentiation and collagen alignment in vitro. J. Cell Sci. *118*, 4731–4739.

Ohl, L., Mohaupt, M., Czeloth, N., Hintzen, G., Kiafard, Z., Zwirner, J., Blankenstein, T., Henning, G., and Forster, R. (2004). CCR7 governs skin dendritic cell migration under inflammatory and steady-state conditions. Immunity *21*, 279–288.

Patel, D.D., Koopmann, W., Imai, T., Whichard, L.P., Yoshie, O., and Krangel, M.S. (2001). Chemokines have diverse abilities to form solid phase gradients. Clin. Immunol. *99*, 43–52.

Podgrabinska, S., Braun, P., Velasco, P., Kloos, B., Pepper, M.S., and Skobe, M. (2002). Molecular characterization of lymphatic endothelial cells. Proc. Natl. Acad. Sci. USA *99*, 16069–16074.

Randolph, G.J., Angeli, V., and Swartz, M.A. (2005). Dendritic-cell trafficking to lymph nodes through lymphatic vessels. Nat. Rev. Immunol. *5*, 617–628.

Rae, J.M., Ramus, S.J., Waltham, M., Armes, J.E., Campbell, I.G., Clarke, R., Barndt, R.J., Johnson, M.D., and Thompson, E.W. (2004). Common origins of MDA-MB-435 cells from various sources with those shown to have melanoma properties. Clin. Exp. Metastasis *21*, 543–552.

Rae, J.M., Creighton, C.J., Meck, J.M., Haddad, B.R., and Johnson, M.D. (2006). MDA-MB-435 cells are derived from M14 melanoma cells—A loss for breast cancer, but a boon for melanoma research. Breast Cancer Res. Treat. Published online September 27. 10.1007/s10549-006-9392-8.

Servant, G., Weiner, O.D., Herzmark, P., Balla, T., Sedat, J.W., and Bourne, H.R. (2000). Polarization of chemoattractant receptor signaling during neutrophil chemotaxis. Science *287*, 1037–1040.

Shields, J.D., Emmett, M.S., Dunn, D.B., Joory, K.D., Sage, L.M., Rigby, H., Mortimer, P.S., Orlando, A., Levick, J.R., and Bates, D.O. (2007). Chemokine-mediated migration of melanoma cells towards lymphatics—A mechanism contributing to metastasis. Oncogene *26*, 2997–3005. Published online November 27, 2006. 10.1038/sj.onc.1210114.

Sipos, B., Kojima, M., Tiemann, K., Klapper, W., Kruse, M.L., Kalthoff, H., Schniewind, B., Tepel, J., Weich, H., Kerjaschki, D., and Kloppel, G. (2005). Lymphatic spread of ductal pancreatic adenocarcinoma is independent of lymphangiogenesis. J. Pathol. *207*, 301–312.

Skobe, M., Hawighorst, T., Jackson, D.G., Prevo, R., Janes, L., Velasco, P., Riccardi, L., Alitalo, K., Claffey, K., and Detmar, M. (2001). Induction of tumor lymphangiogenesis by VEGF-C promotes breast cancer metastasis. Nat. Med. *7*, 192–198.

Soule, H.D., Maloney, T.M., Wolman, S.R., Peterson, W.D., Jr., Brenz, R., McGrath, C.M., Russo, J., Pauley, R.J., Jones, R.F., and Brooks, S.C. (1990). Isolation and characterization of a spontaneously immortalized human breast epithelial cell line, MCF-10. Cancer Res. *50*, 6075–6086.

Stacker, S.A., Caesar, C., Baldwin, M.E., Thornton, G.E., Williams, R.A., Prevo, R., Jackson, D.G., Nishikawa, S., Kubo, H., and Achen, M.G. (2001). VEGF-D promotes the metastatic spread of tumor cells via the lymphatics. Nat. Med. *7*, 186–191.

Takanami, I. (2003). Overexpression of CCR7 mRNA in nonsmall cell lung cancer: Correlation with lymph node metastasis. Int. J. Cancer *105*, 186–189.

Takeuchi, H., Fujimoto, A., Tanaka, M., Yamano, T., Hsueh, E., and Hoon, D.S. (2004). CCL21 chemokine regulates chemokine receptor CCR7 bearing malignant melanoma cells. Clin. Cancer Res. *10*, 2351–2358.

Uchimura, K., Morimoto-Tomita, M., Bistrup, A., Li, J., Lyon, M., Gallagher, J., Werb, Z., and Rosen, S.D. (2006). HSulf-2, an extracellular endoglucosamine-6-sulfatase, selectively mobilizes heparin-bound growth factors and chemokines: Effects on VEGF, FGF-1, and SDF-1. BMC Biochem. *7*, 2.

Wang, J., Zhang, X., Thomas, S.M., Grandis, J.R., Wells, A., Chen, Z.G., and Ferris, R.L. (2005). Chemokine receptor 7 activates phosphoinositide-3 kinase-mediated invasive and prosurvival pathways in head and neck cancer cells independent of EGFR. Oncogene *24*, 5897–5904.

Wiley, H.E., Gonzalez, E.B., Maki, W., Wu, M.T., and Hwang, S.T. (2001). Expression of CC chemokine receptor-7 and regional lymph node metastasis of B16 murine melanoma. J. Natl. Cancer Inst. *93*, 1638–1643.

Williams, C.S., Leek, R.D., Robson, A.M., Banerji, S., Prevo, R., Harris, A.L., and Jackson, D.G. (2003). Absence of lymphangiogenesis and intratumoural lymph vessels in human metastatic breast cancer. J. Pathol. *200*, 195–206.

Wong, S.Y., Haack, H., Crowley, D., Barry, M., Bronson, R.T., and Hynes, R.O. (2005). Tumor-secreted vascular endothelial growth factor-C is necessary for prostate cancer lymphangiogenesis, but lymphangiogenesis is unnecessary for lymph node metastasis. Cancer Res. *65*, 9789–9798.

Yucel, G., and Small, S. (2006). Morphogens: Precise outputs from a variable gradient. Curr. Biol. *16*, R29–R31.

Zigmond, S.H. (1977). Ability of polymorphonuclear leukocytes to orient in gradients of chemotactic factors. J. Cell Biol. *75*, 606–616.